Photoemission spectroscopy using synchrotron radiation. I. Overviews of valence-band structure for Ge, GaAs, GaP, InSb, ZnSe, CdTe, and AgI†

D. E. Eastman and W. D. Grobman
IBM Thomas J. Watson Research Center, Yorktown Heights, New York 10598

J. L. Freeouf* and M. Erbudak
Division of Engineering and Applied Physics, Harvard University, Cambridge, Massachusetts 02138
(Received 17 October 1973)

We determine bandwidths and critical-point positions with respect to the valence-band edge for the valence bands of several extensively studied semiconductors (with an accuracy of about 0.3 eV) by using photoemission densities of states derived from photoemission spectra obtained in the 24–78-eV photon energy range. These photoemission spectra were obtained using synchrotron radiation from an electron storage ring; a double-pass, cylindrical, electrostatic, electron energy analyzer; and samples cleaved and measured *in situ* in ultrahigh vacuum. We give a detailed description of the data-reduction techniques by which electronic state densities and certain valence-band feature positions are determined from photoemission spectra. This description includes a discussion of the effect of various phenomena such as optical-transition-probability variations and Auger-emission peaks. Tables are presented which compare our valence-band-position values with the results of both empirical calculations fit to optical data as well as *ab initio* calculations. We find systematic and significant differences between experiment and calculations fit only to optical data, these differences increasing with crystal ionicity, while *ab initio* calculations generally give a better fit to experiment.

I. INTRODUCTION

In this paper we present photoemission-determined valence-band overviews for several common group-IV, -III-V, -II-VI, and -I-VII semiconductors. From these we determine experimental positions of several band edges or density-of-states critical points with respect to the valence-band edge. The present work presents measurements made in the 15–78-eV photon energy range using synchrotron radiation from the 2.5-GeV storage ring at the Cambridge Electron Accelerator. This work is an extension of previous measurements[1,2] made at lower photon energies. It extends this previous work to additional compounds and, with the higher photon energies used here, represents significant improvements in the determination of the position and shape of features of the lower valence bands. The present paper also presents more extensive discussions of our method[2] for obtaining band positions from photoemission densities of states (PDS's) obtained from photoemission energy distributions (PED's). Furthermore, we discuss the advantages of higher photon energies in helping to distinguish valence-band emission features in the presence of complicating effects such as Auger emission and transition-probability distortions.

The current understanding of the electronic structure of semiconductors away from the gap has been obtained primarily by interpreting optical (including modulation) measurements via model band calculations[3,4] such as those employing the empirical-pseudopotential method[3] (EPM). This procedure, which determines differences in band energies at a given crystal momentum $\vec{k}$ but usually not absolute band-energy locations at different values of $\vec{k}$, is a sensitive probe of the upper valence bands and lowest conduction bands. Our measurements, as well as photoemission data obtained by others as described below, provide new band information which includes the lower valence bands and which, combined with optical data, should provide a guide for refining and testing local and nonlocal empirical-pseudopotential models as well as effective one-electron potentials in "first-principles" calculations such as orthogonalized-plane-wave (OPW) or augmented-plane-wave (APW) calculations.

We observe, as expected, that the upper three valence bands narrow with increasing ionicity, i.e., on going from group-IV (Ge) to group-III-V (GaAs, GaP, InSb) to group-II-VI (ZnSe, CdTe) to group-I-VII (AgI) compounds. Also, as theoretically expected,[3] the lowest (first) valence band is seen to split off from the upper three valence bands for the heteropolar semiconductors (e.g., InSb, CdTe, AgI). EPM calculations fit to optical data consistently obtain widths for the upper three valence bands which are narrower than we observe, and in the case of the II-VI semiconductors (ZnSe, CdTe), these differences become quite large. For example, in Ge the upper two valence bands (E_v-$\Sigma_{1\,\mathrm{min}}$) are 4.5 ± 0.2 eV wide (experiment), while the EPM[5] yields 3.8 eV; in GaAs the corresponding widths are 4.1 ± 0.2 (experiment) and 3.2 eV (EPM)[6]; and in ZnSe the widths are 4.0 ± 0.3 (experiment) and 2.7 eV (EPM).[7] Typically, OPW calculations show

somewhat better agreement with our data for the lower valence bands than EPM calculations fitted to optical data.

Previous photoemission studies[8-10] have usually been limited to photon energies $h\nu \lesssim 11.6$ eV (LiF window cutoff) and have therefore been principally concerned also with states near the gap. To obtain band-structure information from such studies, one usually starts with what one believes is a fairly good model of the over-all band features and positions and then refines it to fit the data better.[8,11-13] However, if the initial band structure chosen is very much in error, then mistaken assignments can be made.[12,13] High-energy overviews such as the ones presented here give directly the correct over-all bandwidths in an unambiguous way and so provide a method of starting with bands which can more easily be refined to fit low-photon-energy photoemission or optical data while minimizing the danger of making errors in assigning observed spectral features to particular optical transitions.

The data most comparable to ours to date are the x-ray-photoemission spectra of Ley *et al.*[14] Their spectra can be compared rather directly with ours to check for possible energy-dependent effects such as transition-probability and sampling-depth effects.

Section II of the present paper gives details of the experimental apparatus. In Sec. III we discuss the nature of the data obtained and the relation of structure in experimental spectra to particular valence-band features of interest here. Section IV presents our data and determines the experimental energy-band positions of interest. These are then compared with the predictions of several theoretical calculations for each of the semiconductors studied. Comparisons with previous experimental data are also presented. Finally, in Sec. V we summarize the results obtained and discuss trends in both the experimental and theoretical calculations on going from the homopolar to heteropolar semiconductors or upon going from one row to another in the Periodic Table.

This paper is the first in a series of papers on photoemission spectroscopy studies of valence bands and core levels using synchrotron radiation. In subsequent papers, we plan to examine many of the group-IV, -III-V, and -II-VI semiconductors in greater depth, as well as describe studies of the noble metals, selected transition metals, transition-metal oxides, transition-metal-layered compounds, rare-earth chalcogenides, actinide compounds, the lead salts, and others. In these papers, we plan to present valence-band overviews, energy-dependent transition probabilities, high-resolution core-level binding energies, spin-orbit splittings, and linewidth measurements, and in selected instances, examine both experimentally and theoretically the "band-structure" regime $h\nu \lesssim 20$–30 eV, for which conservation of crystal momentum as well as energy are important selection rules.

II. DESCRIPTION OF THE EXPERIMENTS

Photoemission spectra were obtained in the range $5 \lesssim h\nu \lesssim 100$ eV using synchrotron radiation from the 2.5-GeV electron storage ring at the Cambridge Electron Accelerator (CEA), Cambridge, Massachusetts.[15-17] A schematic diagram of the experimental system is shown in Fig. 1. An ellipsoidal focusing mirror with a 0.6° grazing angle captures 10 mrad of horizontal beam spread and focuses an image of the source point ($\sim 1 \times 2$ mm) in the storage ring into the user room about 20 m from the source. This mirror can be adjusted remotely and reflects light of all wavelengths λ greater than $\lambda_c \simeq 3.5$ Å, corresponding to all photon energies less than $h\nu_c \simeq 3.5$ keV. Radiation shielding permits occupancy of the user room during all phases of storage-ring operation. With the storage ring operating at 2.5 GeV and 30 mA of dc beam current (typical of our nonparasitic use), the flux of focused radiation is about 10^{14}–10^{15} photons/eV sec in the 10–100-eV range.

A planar beam-splitter mirror with a 2.5-mm-diam hole is used to split the beam for simultaneous operation of an x-ray microscope[18] and our photoemission system. This mirror has a 9° grazing angle and acts as a low-pass filter, i.e., passes only radiation with $h\nu \lesssim 200$–300 eV, so as to avoid x-ray damage to the Au-replica gratings in the monochromators.

Ultrahigh-vacuum (UHV) monochromators ($P \lesssim 1$

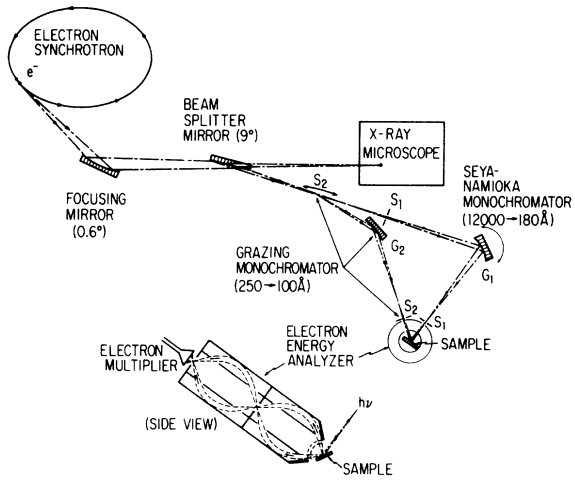

FIG. 1. Schematic diagram of the photoemission system at the CEA 2.5-GeV storage ring (not to scale). The storage ring is ~ 80 m in diameter and the radiation source is about 20 m from the monochromators.

$\times 10^{-9}$ Torr) have been constructed so as not to degrade the vacuum of the sample chamber ($P \lesssim 2 \times 10^{-10}$ Torr). Two monochromators with fixed exit slits have been built, a 1-m Seya–Namioka–type (slits S_1 and grating G_1 in Fig. 1), usable in the 12 000–180-Å range, and a 2-m grazing-incidence-type (slits S_2 and grating G_2), usable in the 250–100-Å range. In order to both maximize efficiency over a wide spectral range and to minimize unwanted higher-order diffraction effects, the Seya-type monochromator has two gratings blazed at ~1200 and 300 Å which can be interchanged *in situ*. This arrangement, together with a LiF filter for wavelengths $\lambda > 1060$ Å, has proven satisfactory for most measurements. Adjustable slits permit the bandwidth $\Delta\lambda$ to be adjusted from $\Delta\lambda = 32$ to 1 Å in the range 12 000–180 Å.

The 2-m grazing-incidence monochromator consists of a fixed exit slit S_2, fixed-position 2400-groove/mm spherical grating blazed at ~120-Å, and a movable entrance slit which consists of a 0.15-mm-wide planar mirror (Au coated) which translates and rotates along the Rowland circle in the path of the photon beam. The bandwidth $\Delta\lambda$ can be varied from about 0.3 to 4 Å throughout the 100–250-Å range.

The monochromatic beams of both monochromators pass through the focal point of the three-stage cylindrical-mirror electron energy analyzer.[19] Samples can be positioned for use with either monochromator by a simple rotation. The cylindrical-mirror analyzer consists of a retard/accelerate stage constructed from two concentric hemispherical grids centered about the sample, followed by a two-stage electrostatic-deflection cylindrical-mirror analyzer (2-in. i.d.) with a Bendix spiraltron electron multiplier. The passband width ΔE (typically 0.1–0.4 eV) is determined by selecting the pass energy $E_p = \Delta E R$, with a resolution of $R \simeq 125$. This analyzer has spatial focusing which permits easy alignment of both monochromators and, by using the hemispherical grid stage to preaccelerate emitted electrons, operates quite well down to zero kinetic energy without spurious secondary emission. In this system counting rates varied monotonically from $\sim 4 \times 10^4$ sec^{-1} at $h\nu \simeq 20$ eV ($\Delta h\nu \simeq \Delta E \simeq 0.2$ eV) to 2×10^3 sec^{-1} at $h\nu \simeq 70$ eV ($\Delta h\nu \simeq \Delta E \simeq 0.4$ eV) when the storage-ring beam current was 30 mA.

Samples were prepared in the form of single crystals of 2×2-mm cross section which were cleaved (with some faceting) and measured *in situ* in the mid-10^{-10}-Torr range. They were oriented for cleaving to produce a (111) surface for Ge and (110) surfaces for the heteropolar zinc-blende compounds. Lightly doped samples were used to avoid complications due to short band-bending depths, since even though $\lesssim 10$ Å below the sample surface is probed in our measurements, extreme degenerate dopings could bend the bands at the surface enough to cause some smearing of structure.

III. CORRESPONDENCE OF PHOTOEMISSION SPECTRAL FEATURES AND VALENCE-BAND POSITIONS

The present section discusses the nature of the correspondence between certain valence-band extrema and one-electron density-of-states critical points, and features in the valence-band photoemission-density-of-states (PDS) overviews. Following sections compare experimental band positions with both those predicted by various theoretical calculations as well as previous experimental results.

A. Relation of spectral features in the density of states to band positions

In order to illustrate the method used to obtain valence-band positions from a PDS, we first show, in Fig. 2, the band structure for Ge calculated using the empirical-pseudopotential model[3] (EPM) and the pseudopotential form factors for Ge given in Ref. 5. Also shown in Fig. 2 is the valence-band density of states $N(E)$ corresponding to this band structure. We note that certain critical points or band minima contribute well-defined edges ($\Sigma_{1\,\mathrm{min}}$, $L_{3'}$, Γ_1) or peaks ($L_1, L_{2'}$) in $N(E)$. This correspondence is not a special feature of Ge, but holds for all homopolar semiconductors, as is shown in calculations similar to this one, but using potentials appropriate to diamond, Si, or grey tin. In the case of the zinc-blende-structure heteropolar semiconductors, the symmetry labels are different[3] and the lowest two bands develop a gap at X. For these semiconductors the features in $N(E)$ corresponding to the upper and lower edges of this gap (denoted by the symmetry labels X_3 and X_1) are relatively sharp edges (see Fig. 7), while the peaks corresponding to L_2 and L_1 in the homopolar semiconductors are no longer well defined. Thus in the heteropolar semiconductors the features corresponding to $L_{3'}$, $\Sigma_{1\,\mathrm{min}}$, and Γ_1 in Ge remain, but are denoted L_3, $\Sigma_{1\,\mathrm{min}}$, and Γ_1, while the lower band features which can be distinguished in $N(E)$ correspond to X_3 and X_1 rather than $L_{2'}$ and L_1.

The basic idea is then to demonstrate that a PDS obtained at high enough photon energy can be expected to reflect the same major peaks and edges as both the calculated $N(E)$ and actual density of states, and so can be used to experimentally determine the position of the major initial points and band minima listed above. Given the proper correspondence between the shape of major features of $N(E)$ and the PDS, this idea works well because the topology of semiconductor band structures is relatively insensitive to the choice of crystal potential,[3] which determines the detailed energy *position*

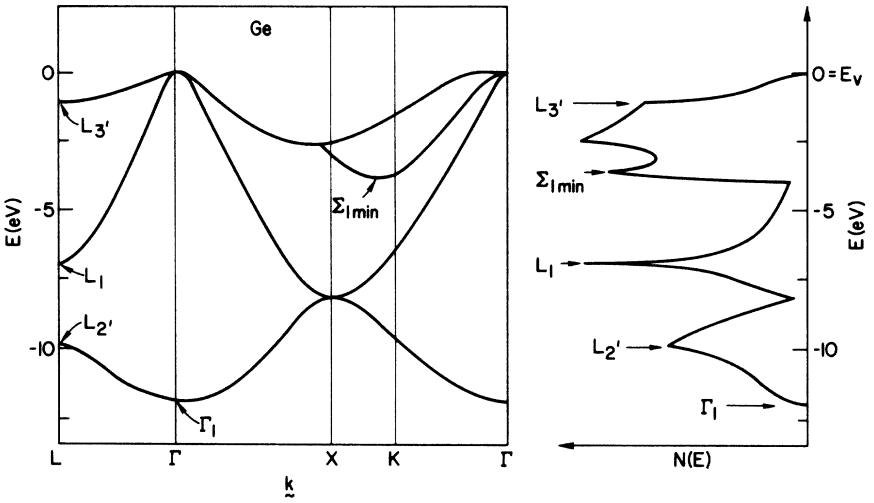

FIG. 2. Valence-band energy E vs crystal momentum $\vec{k}$ in the reduced-zone scheme calculated by the EPM method. Also shown is the one-electron density of states corresponding to this band calculation (taken from Ref. 23). Valence-band critical-point features are indicated both in the energy-band plot and on the density-of-states spectrum. These bands correspond to pseudopotential form factors for Ge given in Ref. 5.

but not the *shape* of the general features of the bands and $N(E)$ described above.

We will now present several experimental and theoretical spectra which illustrate the extent to which major features in $N(E)$ are reflected in photoemission spectra in the presence of the complicating effects of direct transitions, secondary-electron and Auger-electron emission, transition-probability effects, and the short hot-electron-photoemission escape depth.

B. Model calculation of direct-transition effects and secondary-electron emission

In order to consider the extent to which photoemission spectra reflect spectral features in $N(E)$ in the presence of direct-transition effects ($\vec{k}$ conservation during the optical excitation process) and secondary-electron emission, we have performed a model calculation for Ge based on the usual three-step picture of the photoemission process. This calculation is also described in Ref. 2. The starting point was an empirical-pseudopotential-method band calculation of both the valence bands and conduction bands (final states) over the entire energy range involved in 25-eV optical transitions. This calculation used the Cohen–Bergstresser pseudopotential coefficients.[5] The valence-band density of states as well as photoemission spectra were then obtained (including the effect of pseudopotential matrix elements) from a computer program due to Janak[20] which employs a modified version of the Gilat–Raubenheimer[21] k-space integration method. This program assumes direct optical transitions and includes the effects of hole-lifetime broadening, transport to the surface, and escape. The secondary-electron distribution and hole lifetimes were determined using Kane's random-$\vec{k}$ method[22] and fitting to a yield of 1% at $h\nu = 9$ eV. The correlation of structure in the valence-band density of states with that in the calculated photoemission spectra is seen in Fig. 3(a), where we show the primary-, secondary-, and total-electron energy distributions for $h\nu = 25$ eV, as well as the density of states $N(E)$ for this model calculation.

The features in $N(E)$ corresponding to the band edges $L_{3'}$ and $\Sigma_{1\,\mathrm{min}}$, as well as the critical points L_1 and $L_{2'}$, are seen in the primary-photoelectron spectrum in the same positions as in the density of states. Our calculations show that this correspondence is maintained for these features for other values of $h\nu$ in the 20–25-eV energy range. Other features, such as the peak in $N(E)$ at -2.6 eV (near the critical point X_4), change position ($\lesssim 0.4$ eV) in the calculation because of direct-transition effects as $h\nu$ varies. In fact, such changes are also seen experimentally. Structureless secondary-electron distributions, similar to that shown in Fig. 3(a) were calculated for all $h\nu$ in the 20–25-eV range.

The calculation described above indicates that a reasonable over-all view of $N(E)$ can be obtained from a high-energy photoemission energy-distribution curve by subtracting a structureless secondary-electron spectrum of the shape shown in Fig. 3(a) from the total emission curve. Such a procedure is illustrated in Fig. 3(b) for Ge at $h\nu = 25$ eV. The resulting experimental photoemission density of states (PDS) for Ge shows structure attributable to primary emission, and hence the over-all valence-band structure as in the model calculation, but does not include the undesirable skewing caused by secondary-electron emission.

Note that such features as the two deep depressions in the model photoemission spectrum (at about 1.8 and 3.0 eV below E_v), which are direct-transition features, are not seen in the experimental spectrum. That is, the experimental spectra do not contain as strong direct-transition-induced structure as is seen in the model calculation. We

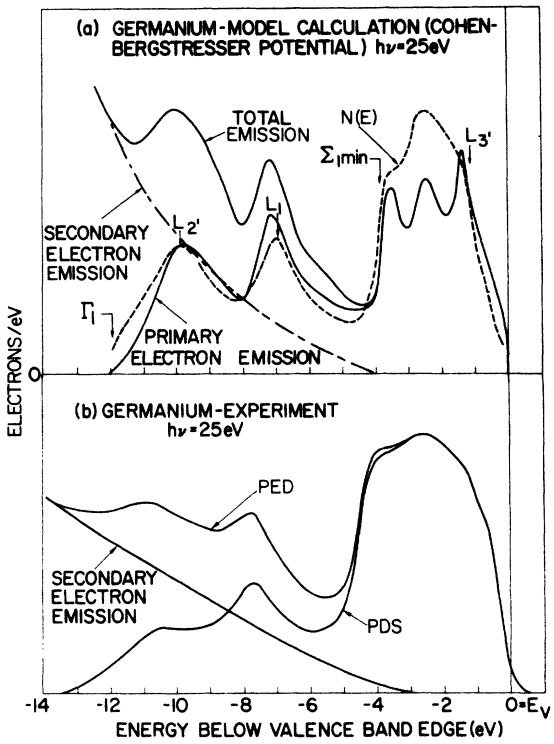

FIG. 3. (a) Comparison between the photoemission primary and total emission for a model calculation for Ge and the density of states $N(E)$ for the same calculation. (b) Illustration of the subtraction of a secondary-electron distribution from a Ge-photoemission energy distribution (PED) to obtain the primary-electron distribution or "PDS." Note that the features in the calculated primary emission in (a) which correspond to one-electron density-of-states features are also seen in the experimental PDS. However, the prominant structure elements in the calculated primary emission which are *not* $N(E)$ features (between ~ -1.2 and 3.6 eV) do not have analogs in the PDS. These features are artifacts of the simplified model, which assumes transitions to nonlifetime or wave-vector-broadened Bloch-like final states. In fact, at these high photon energies, such "joint-density-of-states" features are not seen owing to the final-state lifetime broadening.

believe this is primarily due to the use of nonlife-time-broadened final-state bands in the model calculation. The comparison of experimental spectra for Ge at $h\nu = 25$ and 27.5 eV (in Fig. 4) also shows relatively little direct-transition-induced dispersion of structure. Thus, while the model calculation shows that the spectral features of interest to us are preserved in the presence of direct transitions to sharply defined final bands, the data indicate that such effects are not present to any significant extent in experimental spectra for $h\nu \gtrsim 25$ eV in any event. Experimentally, our procedure in determining when density-of-states features are preserved in the PDS has been to increase $h\nu$ until the features in question become independent of $h\nu$. Generally, we have found it desirable (and sufficient) to obtain overviews in the $25 \lesssim h\nu \lesssim 40$-eV range rather than at higher available energies, $40 \lesssim h\nu \lesssim 100$ eV, since greater intensities (and hence resolution) can be obtained at lower energies. However, in implementing such a procedure, the discussions in Secs. III C and III D below must be kept in mind.

C. Auger emission involving core holes

The Auger emission accompanying photon-produced valence-band holes contributes part of the broad, structureless secondary-electron-emission spectrum which is simply subtracted from a photoemission spectrum to obtain a PDS. However, if $h\nu$ is above threshold for creation of a core hole, then a relatively intense Auger-emission peak can appear superimposed on the primary emission spectrum of interest. (For Ge, such a feature appears at a fixed final-state energy of ~24 eV above E_v owing to "down" transitions from the valence p orbitals into the core hole.) In Fig. 4 we illustrate

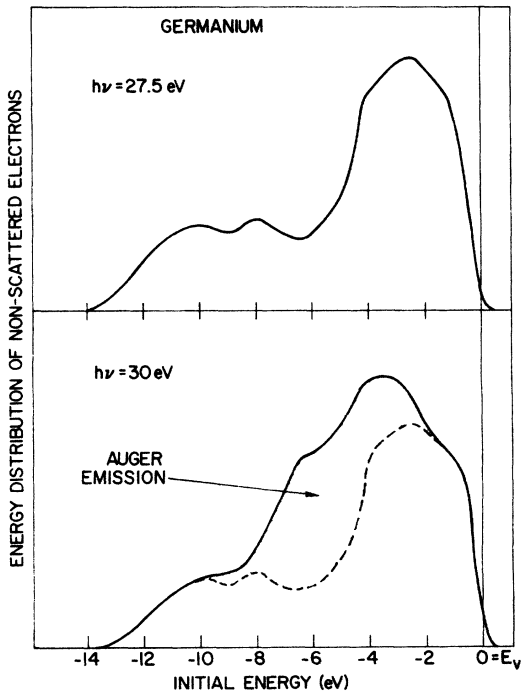

FIG. 4. Comparison of the photoemission primary-electron energy distribution (secondary-electron contribution removed) at $h\nu = 27.5$ eV (below the threshold for Auger transitions) and at 30 eV (above this threshold). In the latter case, the Auger-electron distribution adds to the distribution of electrons emitted from the valence bands (as indicated schematically) to give a total distribution which does not represent a photoemission density of states for the valence bands.

the appearance of such structure by showing photoemission energy distributions for primary-plus-Auger-electron emission (i.e., secondary-electron emission has been subtracted) for Ge obtained at $h\nu = 27.5$ and 30 eV. The threshold for core-hole production in Ge is $h\nu \sim 29$ eV, so the PED at 27.5 eV does not contain an Auger-emission feature as does the PED for 30 eV. The dramatic spectral change in the 30-eV spectrum compared to the 27.5-eV spectrum is due to such Auger emission ($M_{4,5}VV$). Since such emission appears at a fixed final energy, complications due to it can be avoided by operating at a high photon energy ($h\nu \gtrsim 40$ eV in the case of Ge), at which primary valence-band emission occurs at final energies well separated from the Auger emission, or below the Auger threshold ($h\nu \lesssim 29$ eV in the case of Ge).

D. Transition probability and surface effects

Changes in the PDS occur as $h\nu$ changes due to the different photon-energy-dependent transition probabilities for states of different orbital character and/or wave-function extent. Figure 5 compares two photoemission spectra for Ge, a PDS for $h\nu = 25$ eV obtained by us, and a PDS for $h\nu \simeq 1487$ eV obtained[23] by Pollak *et al.* Comparison shows that the lowest two valence-band peaks are excited with slightly greater strengths relative to the upper valence-band peak at $h\nu \simeq 1487$ eV. However, all major peaks and other spectral features appear at the same energy in both spectra with the exception of a shoulder at ~ -0.4 eV seen for $h\nu = 25$ eV, which is due to surface-state emission.[24] This correspondence indicates that transition-probability effects do not affect the apparent energy position of the features of interest. However, at photon energies below 20–30 eV (depending on the material), some of the lower-valence-band features may become very weak. Reference 17 shows this effect in InSb and discusses the need to use high enough photon energies to excite the lower valence bands with significant intensity.

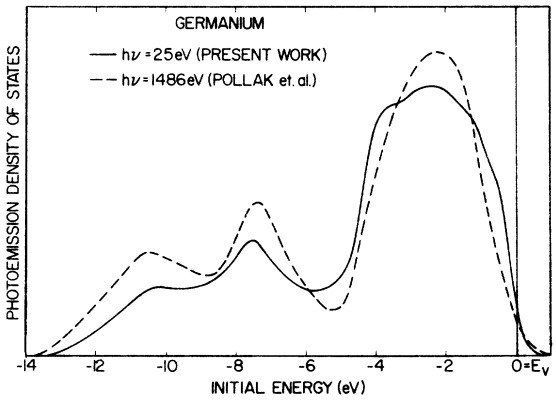

FIG. 5. Comparison of photoemission densities of states for Ge obtained via ultraviolet ($h\nu = 25$ eV) and x-ray ($h\nu = 1486.6$ eV) photoemission spectroscopy. The agreement in energy position of various spectral features is good. At the upper valence-band edge a shoulder is seen in the 25-eV curve which is not seen in the 1486.6-eV curve. This feature is due to surface-state emission which is seen more strongly at 25 eV for a variety of reasons (see text).

Figure 5 also illustrates that in uv-photoemission spectra for $h\nu = 25$ eV, which probe roughly 4–8 Å below the sample surface, we see the same energy states as in the ESCA (electron-spectroscopy-for-chemical-analysis) measurement,[23] which probes roughly 15–30 Å below the surface. Such correspondence indicates that the bulk band structure of single-particle valence-band hole excitations is largely unmodified by surface effects, i.e., is unmodified by the very short probe depth of the short-lived excited electrons which are measured (see Sec. V).

However, owing to the short escape depth in uv-photoemission spectroscopy, we do have high sensitivity to intrinsic surface-state emission and surface-reconstruction effects which appear superimposed on the bulk emission. Such effects have been reported previously,[24] and in the measurements we present here, such emission is seen as a shoulder at -0.4 eV in the PED for Ge (Fig. 2) and is nonobservable for the other materials presented here. That is, for the heteropolar materials we do not see any spectral features which we can associate with surface-state emission; however, such emission could certainly contribute to the spectral intensity.

IV. EXPERIMENTAL PHOTOEMISSION AND VALENCE-BAND STRUCTURES

Selected experimental photoemission distributions (PED's) for GaAs, GaP, InSb, ZnSe, CdTe, and AgI which exhibit main valence-band features are shown in Fig. 6. Data for Ge, for example at $h\nu = 25$ eV, have already been presented in Fig. 3.

After subtraction of the secondary-electron distribution from a PED, the resulting PDS is compared with an empirical-pseudopotential-method (EPM) density of states $N(E)$ in Fig. 7. Figures 7(a)–7(f) present such a comparison for Ge, GaAs, GaP, InSb, ZnSe, and CdTe, respectively. For each material, $N(E)$ was obtained from an EPM calculation[25–27] fit only to optical data. $N(E)$ was convolved with a Lorentzian of half-width Γ varying linearly with energy, from 0.125 eV at the valence-band edge E_v, to 0.375 eV at $E_v - 12$ eV, and the resulting broadened state density is plotted as $N(E)$ in Fig. 7. The broadening simulates that seen in a photoemission experiment due to the apparatus plus that due to finite hole-lifetime effects which

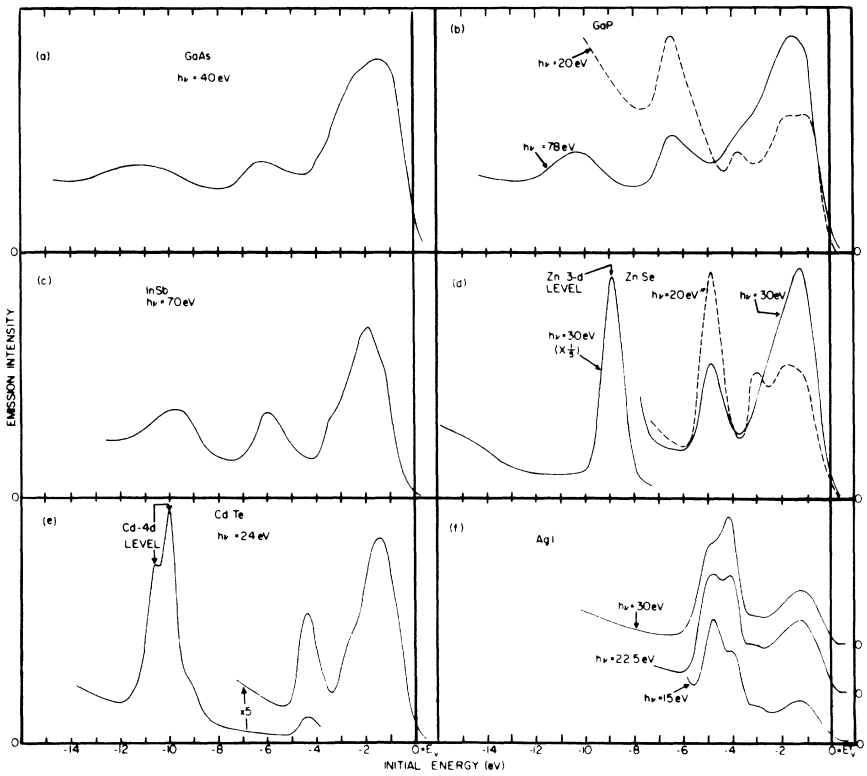

FIG. 6. Photoemission energy distributions (PED's) for several average valence-IV semiconductors. Subtraction of a secondary-electron distribution from these PED's results in the photoemission densities of states (PDS's) given in Figs. 7 and 8. In some cases (e.g., for GaP, ZnSe, and AgI) we also show a spectrum obtained at a relatively low photon energy in order to illustrate the enhancement of the edge corresponding to $\Sigma_{1\,\mathrm{min}}$ (see text).

increase[22] with increasing electron binding energy (i.e., initial energy). The position of various valence-band features obtained from the same EPM calculations used to determine $N(E)$ are shown in Fig. 7. Note that these positions are obtained directly from the EPM calculation itself. The relation of a particular EPM-band critical point to the corresponding spectral feature in $N(E)$ was then used as a guide for determining an experimental valence-band critical point from the corresponding experimental spectral feature in the PDS. Such experimentally determined valence-band critical points are also shown in Fig. 7.

A comparison of theoretical calculations, as well as the results of other experiments, with the data for individual semiconductors is now given, to be followed later by a discussion of general trends. For each semiconductor, the comparison between our results and other experiments and calculations is presented in a table. Of particular interest in each case is the comparison between our results and those of Ley *et al.*,[28] who report x-ray-photoemission-spectroscopy (XPS) measurements at $h\nu = 1486.6$ eV of the valence-band photoemission density of states for cleaved samples in good vacuum. The agreement between our band-position assignments and those of Ley *et al.*[28] is quite good (within ~0.3 eV) in most cases. The agreement between the two independent experiments, represented by the present work, and that of Ley *et al.*,[28] with each data analysis also being performed independently, increases the value of these sets of data as fairly definitive measurements of one-electron energy-band positions in these semiconductors.

Germanium. Comparing the PDS in Fig. 3(b) with the EPM result for $N(E)$ in Fig. 3(a) according to the prescription described above, we obtain experimental values for the band positions $L_{3'}$, $\Sigma_{1\,\mathrm{min}}$, L_1, $L_{2'}$, and Γ_1 of 1.1 ± 0.2, 4.5 ± 0.2, 7.7 ± 0.2, 10.6 ± 0.4, and 12.6 ± 0.3 eV, respectively. All values are measured with respect to the valence-band edge[29] $E_v = \Gamma_{25'} \equiv 0$. The relation of these symmetry labels to valence-band positions is shown in Fig. 2. In Table I, these experimental results are compared with the experimental results of other workers, as well as various theoretical calculations. Note that our experimental value for $\Sigma_{1\,\mathrm{min}}$ was obtained by referring to photoemission distributions obtained at $h\nu \lesssim 20$ eV. Such a procedure was followed for all semiconductors because low-energy PED's (~15 eV) had higher counting rates, better resolution, and enhanced emission intensity for $\Sigma_{1\,\mathrm{min}}$.

We first compare two experiments with our results. Reference 23 gives the x-ray-photoemission density of states ($h\nu = 1486.6$ eV) as well as some band critical-point positions for Ge.

From the first two lines of Table I we see that

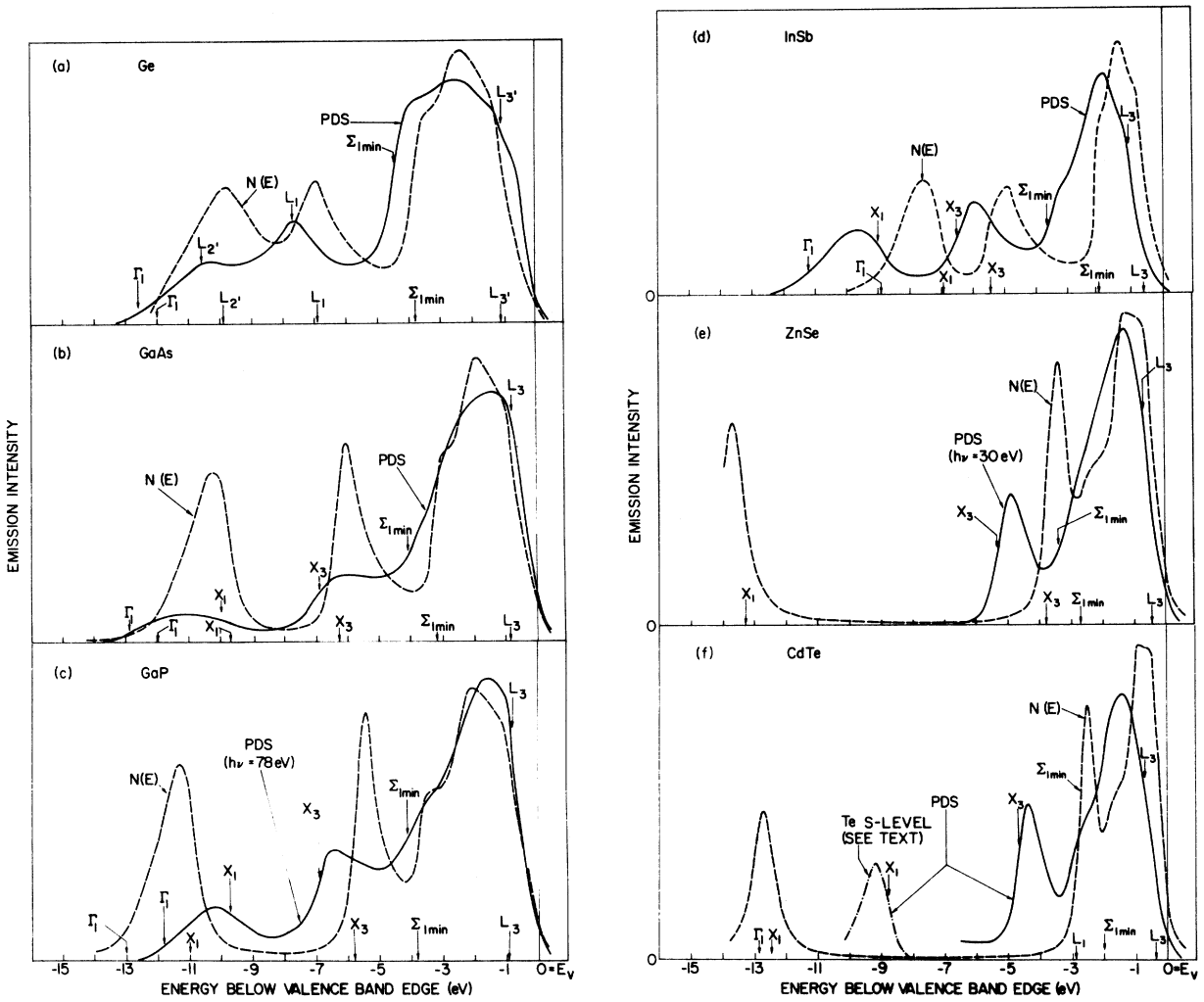

FIG. 7. Comparison of the PDS for six semiconductors with the corresponding EPM-calculation density of states $N(E)$. From such a comparison we can obtain experimental energy-band positions with respect to various spectral features in the PDS curves. Band positions in the EPM calculations are shown using arrows touching the abscissa, while experimental band positions are shown with arrows pointing to the PDS curves.

the critical-point positions L_1, $L_{2'}$, and Γ_1 given in Ref. 23 are in agreement with our values within experimental error. Also, the XPS spectrum presented in Ref. 23 was used in Fig. 5, which compares the corresponding XPS density of states with our PDS. The spectra are in good agreement below -6 eV, while the highest-lying peak (i.e., upper two p bands between 0 and -4.5 eV) has a different spectral shape in the two cases. Emission near $\Sigma_{1\,\mathrm{min}}$ (at -4.5 eV) is weaker in the XPS spectrum owing to transition-probability effects; indeed it is such weakening of emission near $\Sigma_{1\,\mathrm{min}}$ at high photon energies which has led us to use spectra obtained at $h\nu \lesssim 20$ eV to obtain $\Sigma_{1\,\mathrm{min}}$. For Ge, emission near the valence-band edge is more intense in our relatively low-photon-energy photoemission spectrum in Fig. 5. This is due to surface-state emission,[24] which is seen as a shoulder at $\simeq -0.4$ eV. The extrapolations to zero of the upper edge of both spectra fall within 0.1 eV of each other and lie ~0.1 to 0.2 eV above E_v, consistent with our comments in Ref. 29. The over-all agreement between our experimental results for Ge is thus quite good, with the observed differences in spectral shape of the p-band emission between 0 and -4.5 eV being due to transition-probability effects and surface-state emission, as previously mentioned. (These shape differences are also seen in other semiconductors. For example, see our spectra for GaP obtained at $h\nu = 20$ and 78 eV in Fig. 6(b).) Further discussion of the differences between x-ray- and uv-photoemission results is given in Sec. V of this paper.

A low-energy photoemission experiment on Ge,

TABLE I. Experimental and theoretical valence-band energy-state positions for Ge, given as the distance in eV below the valence-band edge. Abreviations for various theoretical methods are EPM, empirical pseudopotential method; adj. OPW, empirically adjusted orthogonalized plane wave; $X_{\alpha\beta}$ OPW method with an exchange approximation using a term in the potential proportional to the charge density to the $\frac{1}{3}$ power and one proportional to the derivative of this quantity; NL, nonlocal.

	$L_{3'}$	$\Sigma_{1\ \mathrm{min}}$	L_1	$L_{2'}$	Γ_1
Experiment[a]	1.1 ± 0.2	4.5 ± 0.2	7.4 ± 0.3	10.6 ± 0.5	12.6 ± 0.3
Experiment[b]	•••	•••	7.2	10.3	13.0
Experiment[c]	(1.4) (1.2)	•••	7.2	•••	•••
Theory[d] ($\vec{k}\cdot\vec{p}$)	1.3	4.0	8.3	11.9	13.5
Theory[e] (EPM)	1.1	3.8	6.9	9.9	12.0
Theory[f] (Fourier series)	1.5	5.3	7.8	8.31	7.3
Theory[g] (adj. OPW)	1.2	4.1	7.4	10.1	12.6
Theory[h] ($X_{\alpha\beta}$ OPW)	1.33	$4.3(\frac{3}{2}X_4)$	7.29	10.48	12.53
Theory[i] (NL pseudopot.)	1.41	4.55	7.51	10.35	12.49
Theory[j] (NL pseudopot.)	1.6	4.8	7.6	10.2	12.4
Theory[k] (OPW)	1.1	3.7	6.7	9.9	11.9

[a]This work ($h\nu=25$ eV) $\Sigma_{1\ \mathrm{min}}$ is obtained from $h\nu<20$-eV spectra (see text).
[b]Reference 23 (using $E_F=E_v$).
[c]Reference 8.
[d]M. Cardona and F. H. Pollak, Phys. Rev. 142, 530 (1966).
[e]Reference 5.
[f]G. Dresselhaus and M. S. Dresselhaus, Phys. Rev. 160, 649 (1967).
[g]Reference 4, relativistic Table I, p. 217.
[h]I. Ortenberger and W. Rudge, IBM Research Report No. RJ-1041 (unpublished).
[i]J. C. Phillips and K. Pandey, Phys. Rev. Lett. 30, 787 (1973).
[j]D. Brust, Phys. Rev. B 4, 3497 (1971), and private communication.
[k]D. J. Stukel *et al.*, Ref. 20, p. 93.

reported by Donovan[30] for $h\nu\lesssim11.6$ eV, was analyzed in Refs. 31 and 32 with values for $L_{3'}$ of -1.4 and -1.2 eV, respectively, which agree fairly well with our value of -1.1 ± 0.1 eV.

Comparing theoretical predictions with our results, we first note that most theoretical densities of states, e.g., $N(E)$ in Fig. 3, have an over-all shape similar to that of our spectra. This observation, which holds for all semiconductors studied, suggests that theoretical band structures such as that in Fig. 2 are correct in the general shape of the bands although bandwidths and gaps may be quantitatively wrong.

Two general types of calculations are represented in Table I, "first-principles" calculations and parametrized calculations which are usually fit to optical data. One calculation is a combination of both methods.

The most popular empirical method, the EPM using a local pseudopotential and fit only to optical data, gets the width of the upper two bands ($E_v-\Sigma_{1\ \mathrm{min}}$) too narrow by 0.7 eV out of 4.5 eV for Ge. This "narrowness" is a common feature of such calculations for all semiconductors studied. If nonlocal terms are added to the pseudopotential, a much better fit to all the valence-band features can be obtained, while maintaining a good fit to fundamental gap and lowest-conduction-band features. This is true for Refs. i and j in Table I, both of which obtain a very good fit to most of the band features we have identified, even though Ref. j was originally fit only to optical data while the calculation in Ref. i adjusted one nonlocal parameter to fit our data, namely, the magnitude of an $l=2$ angular-momentum-dependent nonlocal-potentail term in the Hamiltonian. Also Chelikowsky *et al.*[33] and Shaw[34] have shown that excellent fits to our data for all semiconductors can be obtained using the EPM with a nonlocal "effective-mass" prescription, namely, by changing the electronic mass in the Hamiltonian by typically ~10%, which again involves only one nonlocal parameter.

Results obtained via two other empirical methods fit only to optical data are also listed in Table I, namely, valence-band values obtained by Cardona and Pollak using the $\vec{k}\cdot\vec{p}$ method (Ref. d) and band values obtained by Dresselhaus and Dresselhaus using a Fourier series fit (Ref. f). Both calculations do not agree well with our data, a result which seems largely due to the fact that these calculations were fit to optical data involving only the upper two p bands.

The results of a variety of first-principles calculations are presented in Table I, all based on the

OPW method. The agreement with our band positions varies among these, with rather good over-all agreement seen for the unadjusted $X_{\alpha\beta}$ OPW calculation.

Gallium arsenide. A PED for GaAs ($h\nu = 40$ eV) is given in Fig. 6(a) and the corresponding PDS (with a smooth background of secondary electrons subtracted) is shown in Fig. 7(b), where it is compared with $N(E)$ from an EPM-band calculation.[6] From this comparison we obtain values for L_3, $\Sigma_{1\,\mathrm{min}}$, X_3, X_1, and Γ_1 of 0.8 ± 0.2, 4.1 ± 0.2, 6.9 ± 0.2, 10.0 ± 0.3 and 12.9 ± 0.5 eV, respectively, measured relative to E_v. As previously noted, the p-band edge $\Sigma_{1\,\mathrm{min}}$ was obtained from low-photon-energy data ($h\nu \lesssim 20$ eV).

The over-all shape of the PDS and of $N(E)$ in Fig. 7(b) are again similar, as was the case for Ge. In Fig. 7(b) $N(E)$ shows a gap ($X_3 - X_1$) between the lowest two valence-band peaks. This gap arises in heteropolar semiconductors owing to the lattice-potential asymmetry introduced by the presence of two different ionic species. This gap is also evident in our PDS. Emission in the gap region in the PDS arises in part from the lifetime broadening of the levels near the gap [as is seen for $N(E)$], and in part from uncertainties in subtracting secondary emission from the PED in Fig. 6(a) to obtain the PDS. The latter uncertainty is also enhanced by the weak emission intensity from the lowest two bands at $h\nu = 40$ eV.

In Table II we compare our results with the XPS results of Ley *et al.*[28] The results for the upper three valence bands agree well except for the assignment of L_3. This difference may be due to matrix-element effects or, in part, to the lower resolution (~ 0.6 eV) in the XPS experiment. Such experimental broadening will be most pronounced near E_v, where valence states have small lifetime broadening. The lowest s-like band is different for the two experiments for reasons which are presently not understood. This difference is not seen to this extent in other semiconductors.

The experimental results of Spicer and Eden[8] for L_3 and $\Sigma_{1\,\mathrm{min}}$ in Table II were obtained using $h\nu \lesssim 11.6$ eV and interpreting observed features as being due to direct interband transitions.

Comparisons of band positions with the predictions of various theories are also presented in Table II. The two EPM calculations, which were fit to optical data, give bandwidths for the upper valence bands (i.e., $E_v - \Sigma_{1\,\mathrm{min}}$ and $E_v - X_3$) which are slightly too small, as was the case for Ge. Interestingly, the more recent EPM calculation, which is a refinement of the earlier calculation, since modulation data were also fit, gives poorer agreement with the experimental bandwidth $E_v - \Sigma_{1\,\mathrm{min}}$ than does the older calculation.

In Table II, we also list the results of three first-principles (OPW) calculations. The first is a relativistic, non-self-consistent calculation, while the second ($X_{\alpha\beta}$ OPW) is an improvement over this in which a local exchange correlation potential, depending on both the charge density and its gradient, have been added. The third OPW calculation used an approximate self-consistent potential but is nonrelativistic. All of these calculations have approximated or neglected some features of a complete first-principles calculation, and all of them show agreement with our data comparable with that of the EPM calculations. Again, as in the case of Ge, nonlocal EPM calculations[33,34] in which only one nonlocal parameter (the effective mass) was varied could produce much better fits to photoemission valence-band data than could the local EPM

TABLE II. Experimental and theoretical valence-band positions (eV below the valence-band edge) for gallium arsenide. Abreviations are defined in the caption for Table I.

	L_3	$\Sigma_{1\,\mathrm{min}}$	X_3	X_1	Γ_1
Experiment[a]	0.8 ± 0.2	4.1 ± 0.2	6.9 ± 0.2	10.0 ± 0.3	12.9 ± 0.5
Experiment[b]	1.4 ± 0.3	4.4 ± 0.2	7.1 ± 0.2	10.7 ± 0.3	13.8 ± 0.4
Experiment[c]	1.0	3.8	...	...	...
Theory[d] (EPM)	0.9	3.6	6.15	10.2	12.3
Theory[e] (OPW)	0.9	$3.45(\frac{3}{2}X_5)$	5.5	10.7	12.4
Theory[f] ($X_{\alpha\beta}$ OPW)	1.06	$3.6(\frac{3}{2}X_5)$	6.43	10.24	12.44
Theory[g] (OPW)	1.1	4.0	6.5	9.2	11.8
Theory[h] (OPW)	1.0	3.3	6.2	9.4	11.8
Theory[i] (EPM)	0.9	3.2	6.3	9.7	12.0

[a]This work ($h\nu = 40$ eV).
[b]Reference 28.
[c]Reference 8.
[d]Reference 5.
[e]Reference 4, Table V, column 6.
[f]I. Ortenburger and W. Rudge, IBM Research Report No. RJ-1041 (unpublished).
[g]Reference 20, p. 93 ($\alpha = \frac{2}{3}$).
[h]Reference 20, p. 93 ($\alpha = 1$).
[i]Reference 7.

alone.

Gallium phosphide. PED's for $h\nu = 20$ and 78 eV are shown in Fig. 6(b), and the PDS corresponding to the 78-eV spectrum is shown in Fig. 7(c), along with $N(E)$ obtained from an EPM calculation.[7] The band edges L_3, $\Sigma_{1\,\mathrm{min}}$, X_3, X_1, and Γ_1 are determined to be 0.8 ± 0.2, 4.1 ± 0.3, 6.9 ± 0.3, 9.7 ± 0.3, and 11.8 ± 0.5 eV below the valence-band edge E_v.

In Table III, our results are also compared with the predictions of several band calculations. The agreement with the EPM calculation for the width of the upper two valence bands ($\Sigma_{1\,\mathrm{min}}$) is slightly better for GaP than for GaAs. GaP is an indirect-gap III-V semiconductor, and both the indirect-gap X_1 (conduction band) $-E_v(\Gamma_{15})$ and the $X_1 - X_5$ band separations have been determined from the optical data. Thus the $E_v - X_5$ separation, which is a measure of the width of the upper two valence bands is "built into" the local EPM fit to the optical data. However, some nonlocality must be added to fit all the valence bands as determined by overviews such as presented in this paper.[33,34]

Comparing our results with the x-ray-photoemission-determined band positions[28] given in Table III, we observe excellent agreement for $\Sigma_{1\,\mathrm{min}}$, X_3, and X_1, all determined from relatively sharp edges in the PDS. In the case of L_3 we disagree in the same manner as for GaAs. Since L_3 is determined from a more subtle spectral feature in the same spectrum, the different transition probabilities and resolution of the XPS spectrum may account for the difference. In the case of the bottom of the valence bands, Γ_1, we disagree by about 1 eV (considering the large error bounds). Whether this disagreement is due to the sensitivity of the determination of Γ_1 or to the prescription for subtracting a secondary-electron distribution is yet to be determined.

Indium antimonide. A PED for $h\nu = 70$ eV is shown in Fig. 6(c), and the corresponding PDS as well as $N(E)$ from an EPM calculation[26] are shown in Fig. 7(d). These data were taken at a large value of $h\nu$ with high resolution, and permitted tentative identification of L_2 and L_1 as well as the other band positions determined for GaAs and GaP. We find L_3, $\Sigma_{1\,\mathrm{min}}$, L_2, X_3, X_1, L_1, and Γ_1 to be 1.05 ± 0.2, 3.65 ± 0.3, 5.8 ± 0.3, 6.5 ± 0.3, 9.0 ± 0.3, 10.2 ± 0.3, and 11.2 ± 0.5 eV below E_v. As seen in this figure as well as in Table I, the EPM bands are too narrow, and have a much smaller separation ($X_3 - X_1$) between the first and second valence bands than is observed. Unadjusted OPW calculations (see Table IV) give a better fit to these lower valence bands. In particular, the calculation of Surratt and Collins[35] is significant because it is both relativistic and self-consistent, and thus represents the "best" first-principles calculation available. The agreement between the predictions of this theory and our experimental band positions is good. However, it is not clear how significant this agreement is until additional calculations are performed. This same calculation was applied to ZnSe with poor agreement between the calculated results and optical and photoemission data.[36]

Table IV also gives a comparison of our results with the x-ray-photoemission results of Ley *et al.*[28] The results for all critical points agree to within the combined experimental errors. Again, the XPS value for L_3 is significantly larger than ours.

Zinc selenide. PED's for 20 and 30 eV are shown in Fig. 6(d), and the PDS and an EPM-derived[7] $N(E)$ are shown in Fig. 7(e). Our values for L_3, $\Sigma_{1\,\mathrm{min}}$, and X_3 are 0.7 ± 0.2, 3.4 ± 0.3, and 5.3 ± 0.3 eV below E_v.

We could not obtain values for X_1 and Γ_1 as we observed no emission from the lowest Se-associated s band at the photon energies available to us. The Zn $3d$ level is seen clearly in Fig. 6(d) and its center is about 8.6 eV below E_v. Comparison of the PED's for 20 and 30 eV illustrates the enhancement of states near $\Sigma_{1\,\mathrm{min}}$ at low photon energies.

In Table V, comparison with the XPS data of Ley *et al.*[28] shows that their values are again in good agreement with our results, while the XPS value

TABLE III. Experimental and theoretical valence-band positions (eV below the valence-band edge) for gallium phosphide. Abbreviations are defined in the caption for Table I.

	L_3	$\Sigma_{1\,\mathrm{min}}$	X_3	X_1	Γ_1
Experiment[a]	0.8 ± 0.2	4.1 ± 0.3	6.9 ± 0.3	9.7 ± 0.3	11.8 ± 0.5
Experiment[b]	1.2 ± 0.3	4.0 ± 0.2	6.9 ± 0.2	9.6 ± 0.3	13.2 ± 0.4
Theory[c] (EPM)	0.9	3.9	5.8	11.1	13.1
Theory[d] ($X_{\alpha\beta}$ OPW)	0.9	$3.8(\frac{3}{2}X_5)$	6.0	9.5	12.0
Theory[e] (EPM)	0.9	3.8	5.8	11.0	13.0

[a]This work ($h\nu = 78$ eV).
[b]Reference 28.
[c]Reference 5.
[d]I. Ortenburger and W. Rudge, IBM Research Report No. RJ-1041 (unpublished).
[e]Reference 7.

TABLE IV. Experimental and theoretical valence-band positions (eV below the valence-band edge) for indium antimonide. Abbreviations are defined in the caption for Table I. SCROPW means self-consistent relativistic OPW.

	L_3	$\Sigma_{1\,\min}$	X_3	X_1	Γ_1
Experiment[a]	1.05±0.2	3.65±0.3	6.5±0.3	9.0±0.3	11.2±0.5
Experiment[b]	1.4±0.3	3.4±0.2	6.4±0.2	9.5±0.2	11.7±0.3
Theory[c] (EPM)	0.6	2.3	4.3	8.6	9.8
Theory[d] ($X_{\alpha\beta}$ OPW)	1.05	3.3($\frac{3}{2}X_5$)	5.7	8.6	10.5
Theory[e] (EPM)	0.6	2.1	5.4	6.9	8.9
Theory[f] (SCROPW)	···	3.54	5.9	9.4	10.4

[a]This work ($h\nu$=70 eV).
[b]Reference 28.
[c]Reference 5.
[d]I. Ortenburger and W. Rudge, IBM Research Report No. RJ-1041 (unpublished).
[e]Reference 26.
[f]G. T. Surratt and T. C. Collins, in Ref. 1, p. 959.

for L_3 is again significantly larger than ours. The XPS measurements at $h\nu$=1487 eV were able to observe emission for the Se-associated s level and thus obtain values for X_1 and Γ_1.

As seen in Table V, the EPM results for the upper valence bands ($E_v-\Sigma_{1\,\min}$ or E_v-X_3) are too narrow by several eV. Such a large discrepancy is also seen by us for the other II-VI semiconductor reported here, CdTe. The error in these bandwidths obtained from optically fit EPM calculations is in the same direction as that seen in the III-V semiconductors, but is quantitatively much worse. For this semiconductor, unadjusted OPW calculations come much closer to the proper bandwidth (Table V). These same comments apply to CdTe (see below).

Cadmium telluride. A PED for $h\nu$=24 eV is shown in Fig. 6(e) and the corresponding PDS is compared in Fig. 7(f) with an EPM density of states determined by fitting to optical data.[27] Our experimental widths for the second and third valence bands (e.g., X_3=4.7±0.2 eV and $\Sigma_{1\,\min}$=2.8±0.2 eV) are seen to be much broader than the EPM results (X_3=2.9 eV, $\Sigma_{1\,\min}$=1.9 eV). Also the gap between the first and second bands (X_3-X_1=4.1 eV) is much smaller than the EPM results (X_3-X_1=9 eV). As previously mentioned, this discrepancy in the EPM is largely due to the fact that the EPM was fit only to the upper p bands.

In Fig. 6(e) we also observe the spin-orbit-split Cd 4d levels, at −10.0 ($D_{5/2}$) and −10.65 eV ($D_{3/2}$), respectively, which overlap the first valence band (i.e., Te 5s level) that has an edge X_1 at 8.8±0.3 eV. A PDS feature for the Te 5s level was roughly estimated [see Fig. 7(f)] from the observed emission edge near 9 eV. In this way we roughly estimate Γ_1=10.0±0.5 eV.

Besides the $h\nu$=1486.6-eV overviews of the CdTe valence bands given in Ref. 28 (see Table VI), there are extensive fits[37-39] to low-energy ($h\nu\lesssim$11.6 eV) photoemission data[40] in the literature. In all of the previous theoretical studies, the starting band model assumes that the total width of the upper three valence bands (E_v-X_3) is ~3 eV, while the data of the present paper and Ref. 28 give a total width of the upper three bands of ~5 eV. Since the

TABLE V. Experimental and theoretical valence-band positions (in eV below the valence-band edge) for zinc selenide. Abbreviations are given in the caption for Table I.

	L_3	$\Sigma_{1\,\min}$	X_3	X_1	Γ_1
Experiment[a]	0.7±0.2	3.4±0.3	5.3±0.3	···	···
Experiment[b]	1.3±0.3	3.4±0.2	5.6±0.3	12.5±0.4	15.2±0.6
Theory[c] (EPM)	0.51	2.6	3.7	13.3	14.1
Theory[d] (SCOPW)	0.8	3.1	4.9(L_{1v})	10.3	11.8
Theory[e] (SCOPW)	0.75	2.7	4.4	10.5	11.8
Theory[f] (OPW)	···	2.47($\frac{3}{2}X_5$)	4.3	10.5	11.8
Theory[g] (EPM)	0.45	2.7	3.8	13.3	14.2

[a]This work ($h\nu$=30 eV).
[b]Reference 28.
[c]Reference 5.
[d]Reference 20, p. 93 ($\alpha=\frac{2}{3}$).
[e]Reference 20, p. 93 (α=1).
[f]Stukel *et al.*, Phys. Rev. 179, 740 (1969).
[g]Reference 7.

TABLE VI. Experimental and theoretical valence-band positions (in eV below the valence-band edge) for cadmium telluride. Abbreviations are given in the caption for Table I.

	L_3	$\Sigma_{1\,\min}$	X_3	X_1	Γ_1
Experiment[a]	0.7±0.2	2.8±0.2	4.7±0.2	8.8±0.3	···
Experiment[b]	0.9±0.3	2.7±0.3	5.1±0.2	···	···
Experiment[c]	0.7	1.9	3.1(L_1)	···	···
Theory[d] (EPM)	0.4	1.9	2.9	11.9	12.4
Theory[e] (ROPW)	0.75	2.3($\frac{3}{2}X_5$)	3.9	9.6	10.4
Theory[f] (EPM)	0.4	2.5	3.15	···	···

[a]This work ($h\nu$=24 eV).
[b]Reference 28.
[c]Reference 13.
[d]Reference 5.
[e]J. P. Van Dyke and F. Herman, ARL Report No. 69-0080, Sec. 19 (unpublished).
[f]Reference 27.

starting points for the studies in Refs. 37–39 were significantly in error, the fits obtained by these authors to the low-energy photoemission data[40] were misleading. However, given starting bands with the correct bandwidths, such as the calculations in Refs. 33 and 34, which are fit to high-energy overviews, low-energy data[40] could be reexamined and used to obtain a more detailed picture of the energy bands for CdTe.

From Table VI we see that, as with ZnSe, unadjusted OPW calculations give[1] a more accurate picture of the valence bands than the EPM fit to optical data. In both cases, the Cd 4*d* level is not included in the calculations. Also, as previously discussed, nonlocal EPM calculations can give good fits to both optical data and high-energy photoemission data.

Silver iodide. Figure 6(f) shows PED's for AgI for photon energies $h\nu$=15, 22.5, and 30 eV. As there are no published band structures for this material, we can only point out the main features and reason by analogy with its row-5 partners (InSb and CdTe). Interpretation of these spectra is further complicated by the position of the Ag 4*d* levels, whose upper edge lies only 4 eV below E_v, and in fact slightly overlaps the second valence band.

In contrast with the cation *d* levels in the III-V and II-III semiconductors, the Ag *d* levels in AgI form bands (of width ~2 eV) rather than atomiclike levels. This is demonstrated by the strong variation of the ratio of the two Ag *d*-derived peaks (at 4.15 and 4.9 eV below E_v) with photon energy, an effect not observed in the In or Cd compounds previously discussed. The proximity of the Ag 4*d* levels to the upper three valence bands indicates strong mixing of the *d* bands and the valence bands, and thus modifies the valence-band structure of AgI compared with that of InSb or of CdTe. In light of this probable mixing, and the hexagonal crystal structure, the upper three valence bands of AgI need not have the same critical-point order as InSb and CdTe. Nevertheless, the valence-band spectra are similar, and we therefore use the same labels for valence-band edges, as summarized in Table VII.

The value for X_3 shown in Table VII is obtained by assuming that the band-two edge lies below the peak by the same amount that it lies below the corresponding peak in photoemission spectra we have obtained for hexagonal ZnO, where *d*-*p* mixing also occurs. The assignment of the value for X_1 is tentative since the lowest-lying valence-band peak (see Fig. 8) is ~4 eV wide, much wider than one would expect for the I *s* level. Complications such as *s*-*d* mixing, an unusually short hole lifetime, or a characteristic energy-loss peak below the Ag *d* level might affect the width of this peak.

From Table VII we observe that the width of the upper three valence bands is 3.7 eV, and the gap between the first and second valence bands ($X_3 - X_1$) is ~6.1 eV. As band calculations for AgI have not been performed, we simply note the relation of our 3.7-eV width for the upper three valence bands of AgI with the theoretical widths for these bands for

TABLE VII. Experimental valence bands and Ag *d*-level positions in silver iodide (in eV below the valence-band edge).

	L_3	$\Sigma_{1\,\min}$	X_3	X_1	Γ_1	$d_{5/2}$	$d_{3/2}$
Experiment[a]	···	2.4±0.2	3.7±0.4	9.8±1.0	···	4.15±0.1	4.9±0.1
Experiment[b]	···	···	···	···	···	4.4	···

[a]This work ($h\nu$=22.5 eV).
[b]Reference 43.

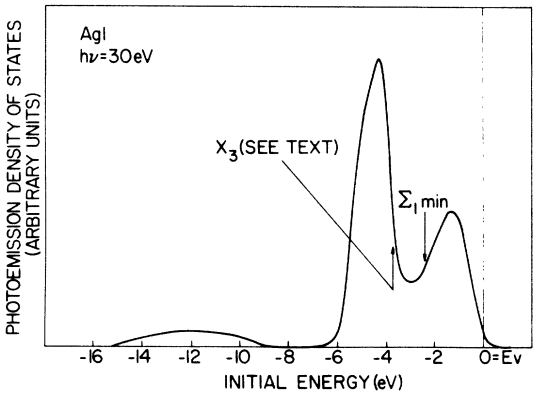

FIG. 8. PDS curve for AgI.

AgCl and CuI, which are 3.4 (tight binding),[41] and 2.8 eV (LCAO-OPW),[42] respectively. Both values are less than for the AgI bands measured in our experiment. Low-energy ($h\nu < 12$ eV) photoemission measurements have been performed on evaporated films of AgI by Bauer (Ref. 43). He observed the strong p-derived peak near E_v corresponding to bands 3 and 4, and observed the d-derived structure at ~ -4.4 eV.

V. DISCUSSION

This summary section discusses agreement between the work of others and the present paper, compositional trends and features common to all of our spectra, and applications of the results of this paper.

The first important feature we note is the good agreement between x-ray photoemission studies[23,28] and the present results. From Tables I–VI we see that x-ray[23,28] and the present uv-photoemission studies ($h\nu \lesssim 80$ eV) give results for the position of $\Sigma_{1\,\mathrm{min}}$, X_3, X_1, L_1 (Ge), and $L_{2'}$ (Ge) with respect to E_v which agree on average within ~ 0.25 eV. That is, for the band features which manifest themselves as sharp edges or peaks, these two separate and independent studies agree very well even though there are differences in transition probabilities, escape depths for emitted electrons, experimental resolution, and detailed prescriptions for associating spectral features with valence-band positions.

The fact that these photoemission valence-band results are independent of the escape depth illustrates an important point, namely, that structural features of a bulk-associated density of states are seen in photoemission.[47] This is due to the fact that the relevant valence-band *hole* states are distributed in energy in a manner determined by long-range crystal electronic structure even though the final *electron*-state wave function is localized near the surface. More precisely, the optical transitions producing emitted electrons occur between bulklike initial states with long coherence lengths (arising from the long hole lifetime) and excited states which have a short extent (~one escape depth) within the solid.[47] Thus main features in the spectral density of bulk valence states are seen in the emitted electron distribution, the surface primarily affecting transition probabilities. Of course the short penetration of the final-state wave function into the solid enhances the extent to which states which are surface associated (i.e., intrinsic surface states) are seen. Their emission then appears superimposed on that coming from bulklike initial states.[24]

In the case of L_3 the XPS studies[28] always place L_3 further below E_v than does UPS, by an amount which averages ~ 0.4 eV. We believe that our results for L_3 are more accurate, since the lower XPS resolution (~ 0.6 eV vs typically 0.025–0.45 eV for our spectra) will most strongly affect states near E_v, which are inherently much sharper (i.e., longer lived) than lower-energy valence-band states. For this reason the subtle spectral feature associated with L_3 is probably less precisely determined by XPS.

The bottom edge of the valence bands, at Γ_1, is consistently lower in XPS than in our work, by an average of about 0.8 eV. The lower edge of the valence bands is manifested in an edge which is not sharp, owing in part to shorter lifetimes for hole states far away from E_v. This edge is superimposed upon the secondary-electron energy distribution, which must be subtracted to obtain the PDS. The difference between this subtraction in Refs. 23 and 28 compared to the present paper, coupled with other differences, such as the prescription for obtaining the edge and the differing experimental resolutions, could result in this discrepancy. The over-all agreement between UPS and XPS is thus generally better than ~ 0.4 eV, with sharp valence-band features usually in somewhat better agreement.

In contrast, previous low-photon-energy studies have sometimes been interpreted as indicating bandwidths which disagree with ours by as much[37–39] as ~2 eV for CdTe.[40] As noted previously, this large disagreement arises from the fact that the starting energy bands from which the results of Refs. 37–39 were obtained were in error by several eV. This indicates one important use of the present work. Namely, it provides bandwidths and critical points which can be used to distinguish between various valence-band calculations, e.g., effective potentials, etc. Starting with a calculation in agreement with our present results, it should then be fruitful to calculate photoemission spectra at low photon energies, $h\nu \lesssim 20$ eV, and compare with experimental data in order to determine more details of the energy bands for various materials.

We have seen that our over-all PDS shapes were

quite similar to those of $N(E)$ determined using the EPM (see Fig. 7), but that widths for the upper three valence bands ($E_v - X_3$) were consistently greater than determined via the EPM based on optical data alone. Furthermore, this disagreement is largest for the most ionic II-VI compounds. Tables I–VI show that the discrepancy is generally reduced for "first-principles" calculations. While there are difficulties in attempting to use the EPM with a local potential to fit our data, the EPM with one nonlocal parameter can fit both our new data and optical data.[33,34]

One important trend seen both in empirical and first-principles calculations (see the references in Table I–VI) is the widening of the gap between bands 1 and 2 (the lowest two valence bands) and the decreasing of the total width of bands 2–4 ($E_v - X_3$) as one goes from the covalent homopolar group-IV compounds to the heteropolar III-V compounds and then the more ionic II-VI and I-VII compounds. The densities of states in Fig. 7 show this trend for the experimental PDS (solid curves) and the EPM state density (dashed curves). The experimental trends for the compounds studied here are shown in Fig. 9, where we plot $E_v - \Sigma_{1\,\min}$ and $X_3 - X_1$ as a function of increasing ionicity keeping the row of the Periodic Table constant (e.g., as one goes from Ge to GaAs to ZnSe).

The increase in the gap $X_3 - X_1$ as ionicity increases has previously[45,46] been related to one of the parameters C of the Phillips–Van Vechten dispersion theory[43] of ionicity in crystals having an average valence of four. As discussed in Refs. 45 and 46, we have found that $X_3 - X_1 \simeq C$. In the theory, C is a measure of the fraction of the total bond energy in the crystal associated with ionic energy. The agreement between $X_3 - X_1$ obtained from PDS curves and the parameter C, which was determined from other data,[47,48] is significant for two reasons. First, because it suggests that C determined by dispersion theory is significant in predicting crystal properties beyond the scope of the original theory, and secondly because it suggests at least one way in which we can rather directly determine from high-energy photoemission spectra parameters related to the chemical-bond nature of these materials.

Our experimental energy-band positions in Tables I-VI comprise a reliable set of absolute energy positions for testing "first-principles" band calculations in these crystals as well as for use in fitting empirical-band-calculation schemes such as the EPM. Furthermore, optical data yielding $\epsilon_2(\omega)$ give the positions of various conduction-band features with respect to the valence-band features studies here. Thus, the combination of $\epsilon_2(\omega)$ data and photoemission PDS curves can be used for testing calculations of both occupied and unoccupied bands. The combination of both sets of data will then aid in determining the range of validity of one-electron theory and the relation between ground-state and excited-stated properties.

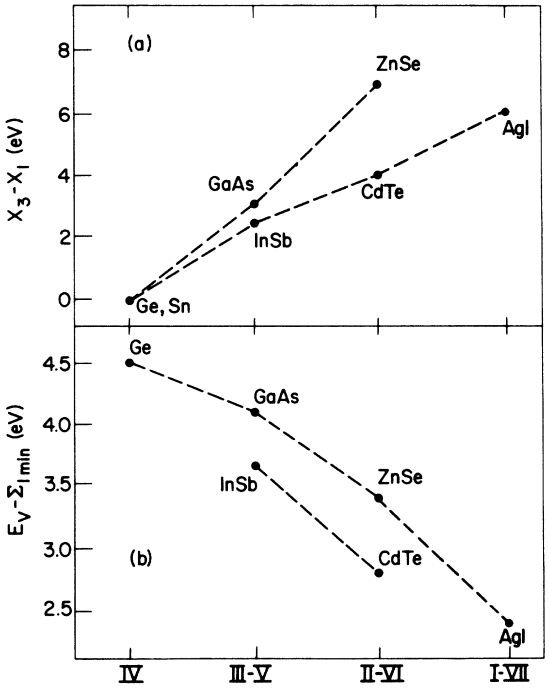

FIG. 9. In (a) and (b), respectively, we plot the ionicity gap ($X_3 - X_1$) and width of the upper valence bands ($E_v - \Sigma_{1\,\min}$) as a function of valence difference for the constituents of average valence-IV compounds in rows 4 and 5 of the Periodic Table. The value for ($X_3 - X_1$) for ZnSe was obtained from Ref. 28.

ACKNOWLEDGMENTS

We are grateful to R. A. Pollak for many helpful discussions, and to D. J. Chadi and Marvin L. Cohen for supplying us with $N(E)$ curves used in Fig. 7. We wish also to thank W. Paul and the staff at the Cambridge Electron Accelerator. Finally, we thank D. C. Reynolds and H. K. Henisch for providing some of the single crystals discussed herein.

†Supported in part by the Air Force Office of Scientific Research under Contract No. F44620-70-C-0089, the National Science Foundation under Grant No. GH35823 and the Atomic Energy Commission under Contract No. AT(11-1)3063.

*Present address: IBM Thomas J. Watson Research Center, Yorktown Heights, N.Y. 10598.

[1]D. E. Eastman and W. D. Grobman, *Proceedings of the*

Eleventh International Conference on the Physics of Semiconductors (Polish Scientific, Warsaw, 1972), p. 12–15.

[2]W. D. Grobman and D. E. Eastman, Phys. Rev. Lett. 29, 1508 (1972).

[3]A comprehensive review of the EPM is presented by M. L. Cohen and V. Heine, in *Solid State Physics*, edited by H. Ehrenreich, F. Seitz, and D. Turnbull (Academic, New York, 1970), Vol. 24, pp. 38–249.

[4]Empirically adjusted OPW calculations are described by F. Herman *et al*, in *Methods In Computational Physics*, edited by B. Alder, S. Fernbach, and M. Rotenberg (Academic, New York, 1968), Vol. 8, pp. 193–250.

[5]M. L. Cohen and T. K. Bergstresser, Phys. Rev. 141, 789 (1966).

[6]R. L. Zucca, J. P. Walter, Y. R. Shen, and M. L. Cohen, Solid State Commun. 8, 627 (1970). A pseudopotential coefficient $V_s(8) = -0.0008$ Ry was used rather than -0.008 Ry, which was misprint in this reference.

[7]J. P. Walter and M. L. Cohen, Phys. Rev. 183, 763 (1969).

[8]A comprehensive review of many of these studies is given in W. E. Spicer and R. C. Eden, in *Proceedings of the Ninth Internal Conference on the Physics of Semiconductors* (Nauka, Moscow, 1968), p. 65. Also see the references listed under 9 and 10 below.

[9]References to $h\nu \lesssim 11.6$-eV studies of GaAs and Ge are also given in W. E. Spicer, J. Res. Natl. Bur. Stand. (U.S.) A 74, 397 (1970).

[10]Early studies of Si and Ge were reported in F. G. Allen and G. W. Gobeli, Phys. Rev. 144, (1965). An extensive study of CdTe is given in Ref. 40 below.

[11]L. R. Saravia and L. Casamayou, J. Phys. Chem. Solids 32, 1075 (1971); 32, 1541 (1971).

[12]L. R. Saravia and L. Casamayou, J. Phys. Chem. Solids 33, 145 (1972).

[13]J. L. Shay, W. E. Spicer, and F. Herman, Phys. Rev. Lett. 18, 649 (1967).

[14]See Ref. 28.

[15]Previously, similar studies have been made in the energy range $5 \lesssim h\nu \lesssim 40$ eV, using synchrotron radiation at the Physical Sciences Laboratory, Stoughton, Wisconsin. For example, see D. E. Eastman and W. D. Grobman, Phys. Rev. Lett. 28, 1327 (1972).

[16]D. E. Eastman, J. Freeouf, and M. Erbudak, in Proceedings of the Congress for the Centenary of the Societe Francaise de Physique, Vittel, France, 1973, to be published in J. Phys. (Paris).

[17]D. E. Eastman and J. Freeouf, Solid State Commun. (to be published).

[18]Paul Horowitz and John A. Howell, Science 178, 608 (1972).

[19]Properties of the cylindrical, electrostatic, mirror electron energy analyzer are discussed in H. Z. Sar-El, Rev. Sci. Instrum. 38, 1210 (1967); 42, 810 (1971).

[20]Algorithms for computing photoemission distributions are described in J. Janak *et al.*, *Electronic Density of States*, edited by L. H. Bennett, Natl. Bur. Stand. (U.S.) Spec. Publ. 323 (U.S. GPO, Washington, D. C., 1971), p. 181.

[21]G. Gilat and L. P. Raubenheimer, Phys. Rev. 144, 390 (1966).

[22]E. O. Kane, Phys. Rev. 159, 624 (1967).

[23]R. A. Pollak *et al.*, Phys. Rev. Lett. 29, 1103 (1972); L. Ley *et al.*, Phys. Rev. Lett. 29, 1088 (1972).

[24]D. E. Eastman and W. D. Grobman, Phys. Rev. Lett. 28, 1378 (1972).

[25]EPM state densities [$N(E)$ in Fig. 7] were supplied by D. J. Chadi and Marvin L. Cohen. They were obtained from band calculations using pseudopotential form factors for Ge, GaAs, GaP, InSb, ZnSe and CdTe obtained from Refs. 5, 6, 7, 26, 7, and 27, respectively.

[26]C. Varea de Alvarez *et al.*, J. Chem. Phys. Solids. (to be published).

[27]D. J. Chadi *et al.*, Phys. Rev. B 5, 3058 (1972).

[28]L. Ley, R. A. Pollak, F. R. McFeely, S. P. Kowalczyck, and D. A. Shirley, Phys. Rev. B (to be published).

[29]For InSb, we obtained the position of E_v from the known value of $E_F - E_v$. For several of the other semiconductors discussed in this paper, the $E_F - E_v$ separation is uncertain owing to band bending (i.e., surface states). Consequently, we have determined E_v by extrapolating the high-energy edge of the valence-band PED to zero intensity and then placing E_v about 0.1 eV below this point of zero intensity (the latter is meant to empirically account for our finite resolution). We estimate that this procedure introduces an uncertainty in E_v of $\lesssim \pm 0.1$ eV in most cases.

[30]T. M. Donovan, Ph. D. thesis (Stanford Univ., 1970) (unpublished).

[31]See Ref. 8.

[32]L. R. Saravia and L. Casamayou, J. Phys. Chem. Solids 32, 1541 (1971).

[33]J. Chelikowsky, D. J. Chadi, and Marvin L. Cohen, Phys. Rev. B (to be published).

[34]J. C. Phillips and K. C. Pandey, Phys. Rev. Lett. 30, 790 (1973); and J. Shaw (private communication).

[35]G. T. Suratt and T. C. Collins, in Ref. 1.

[36]T. C. Collins (private communication).

[37]F. Herman, R. L. Kortum, C. D. Kuglin, and R. A. Short, in *Quantum Theory of Atoms, Molecules and the Solid State*, edited by P. O. Löwdin (Academic, New York, 1966), p. 381.

[38]See Ref. 13.

[39]See Ref. 12.

[40]J. L. Shay and W. E. Spicer, Phys. Rev. 161, 799 (1967).

[41]F. Bassani, R. S. Knox, and W. Beall Fowler, Phys. Rev. 137, A1217 (1965).

[42]Kong-Sop Song, J. Phys. Chem. Solids 28, 2003 (1967).

[43]R. S. Bauer, Ph. D. thesis (Stanford Univ., 1970) (unpublished).

[44]P. Feibelman (unpublished).

[45]W. D. Grobman, D. E. Eastman, and Marvin L. Cohen, Phys. Lett. A 43, 49 (1973).

[46]D. J. Chadi, Marvin L. Cohen, and W. D. Grobman, Phys. Rev. B (to be published).

[47]J. C. Phillips, Rev. Mod. Phys. 42, 317 (1970).

[48]J. A. Van Vechten, Phys. Rev. 182, 891 (1969).